Electromagnetic Stirring in Crystal Growth Processes

Nancy Ma[1] and John S. Walker[2]

Abstract: For semiconductor crystal growth from a melt, stirring due to the interaction of a steady electric current and a steady magnetic field can lead to a more uniform distribution of the additives in the crystal. This paper treats the electromagnetic stirring in a cylinder with a weak uniform axial magnetic field and with an electric current between an electrode in the center of the top of the cylinder and an electrode at the vertical wall of the cylinder. The magnitude and distribution of the stirring are studied as functions of the aspect ratio of the cylinder and of the strength of the electromagnetic body force. All of the steady axisymmetric flows considered here are stable with respect to small perturbations.

1 Introduction

In the vertical gradient freeze (VGF) method, a single crystal grows vertically upward through the solidification of a melt contained in a vertical cylindrical ampoule (Monberg, 1994). Ostrogorsky and Muller (1994) showed that the use of a submerged heater in the VGF method leads to a more uniform axial distribution of the additives in the crystal. A submerged heater is a circular disk, whose diameter is slightly less than the inside diameter of the ampoule. Placed in the melt, the submerged heater separates an upper melt region above the heater from a lower melt region between the heater and the crystal. The submerged heater is raised as the crystal grows, so that the axial height of the lower melt region is constant. Melt flows from the upper melt region, through the narrow radial gap between the periphery of the heater and the ampoule wall, and into the lower melt region. While the submerged heater leads to greater axial uniformity of the additives in the crystal, it may lead to large radial variations, because the melt with low concentrations of the additives enters the lower melt region near the periph-

ery of the crystal-melt interface. This radial macrosegregation can be eliminated through electromagnetic (EM) stirring (Ma et al., 2003). For EM stirring, a graphite rod through the center of the fused silica heater disk acts as one electrode and a cylindrical graphite liner inside the ampoule acts as another electrode. A solenoid around the crystal growth furnace produces a weak uniform axial magnetic field. The interaction of the steady electric current between the two graphite electrodes and the magnetic field drives a steady axisymmetric azimuthal melt motion. The axial variation of the centrifugal force due to the azimuthal velocity drives a steady axisymmetric meridional melt motion with radial and axial velocity components. The meridional circulation provides the mixing in the melt, which leads to more uniform additive distributions in the crystal.

In a crystal growth process, the melt motion driven by the EM body force is coupled to the buoyant convection and the flow from the heater-ampoule gap to the crystal-melt interface (Ma et al., 2003; Wang et al., 2006). Here we isolate the EM stirring in order to study the characteristics of this flow as functions of the aspect ratio of the lower melt region and of the magnitude of the EM body force. The flow driven by a steady electric current and a steady magnetic field is closely related to the flow driven by a rotating magnetic field (RMF). The uses of RMF's in crystal growth processes were reviewed by Dold and Benz (1999). The linear stability analysis for the flow driven by an RMF in a cylinder was presented by Grants and Gerbeth (2002). The differences between the present flow and that driven by an RMF arise from the differences between the azimuthal EM body forces. First, for an RMF, the azimuthal body force varies roughly as the radial coordinate r, but here the body force varies roughly as $1/r$ between the two electrodes. Second, for an RMF, the body force is symmetric about a plane, which is midway between the top and bottom of the cylinder, but here the body force is far from symmetric with a much stronger force near the top boundary.

EM stirring has also been used during the Czochralski

[1] Department of Mechanical and Aerospace Engineering, North Carolina State University, Campus Box 7910, Raleigh, NC 27695, USA

[2] Department of Mechanical and Industrial Engineering, University of Illinois, 1206 West Green St., Urbana, IL 61801, USA
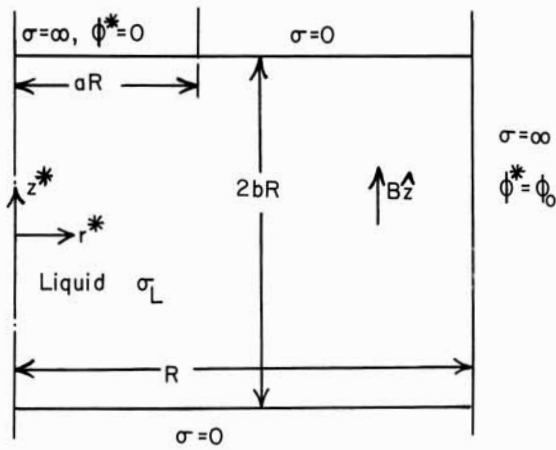
Figure 1 : Dimensionless geometry with the electrical conductivities σ and the weak uniform axial magnetic field $B\hat{\mathbf{z}}$.

growth of silicon crystals (Watanabe et al., 1999; Watanabe et al., 2002). In the Czochralski process, the melt is contained in an open crucible and the crystal grows from the central region of the top of the melt. In the experiments of Watanabe et al. (2002), the crystal served as one electrode and a small electrically conducting rod was inserted into the free surface at one azimuthal position near the crucible wall to serve as the second electrode. The electric current is concentrated near the azimuthal plane where the second electrode enters the melt. Therefore the EM body force and the resultant melt motion are very far from axisymmetric, so that there is no relationship to the axisymmetric flow treated here.

2   Problem formulation

The dimensional geometry is sketched in Fig. 1. The cylindrical liquid region has a radius R and an axial dimension $2bR$. The top boundary at $z* = bR$ consists of the bottom of the graphite rod for $r* \leq aR$ and of the bottom of the fused silica heater for $aR \leq r* \leq R$, where r, θ, z are cylindrical coordinates, and an asterisk denotes a dimensional variable. The bottom boundary of the liquid at $z* = -bR$ is the crystal-melt interface, while the vertical boundary at $r* = R$ is the inside surface of the graphite liner. Both the fused silica and the crystal have electrical conductivities, which are much less than the electrical conductivity σ_L of the liquid, so that they can be treated as electrical insulators with $\sigma = 0$. The electrical conductivity of graphite is much greater than σ_L,

so that the two electrodes can be treated as perfect electrical conductors with $\sigma = \infty$. The weak uniform axial magnetic field produced by the external solenoid is $B\hat{\mathbf{z}}$, where B is the magnetic flux density, and $\hat{\mathbf{r}}, \hat{\theta}, \hat{\mathbf{z}}$ are unit vectors for the cylindrical coordinates. The dimensional voltage difference between the two electrodes is ϕ_0.

In addition to the axial magnetic field produced by the external solenoid, there is an azimuthal magnetic field produced by the electric current between the two electrodes. The interaction of the azimuthal magnetic field and the electric current produces an EM body force which has radial and axial components and which is exactly balanced by a pressure gradient, so that it does not drive any flow. In Ohm's law, the characteristic ratio of (1) the induced electric field due to the flow across the magnetic field lines to (2) the static electric field due to the voltage difference between the electrodes is the interaction parameter

$$N = \left(\frac{\sigma_L B^3}{\rho \phi_0} \right)^{1/2} R, \tag{1}$$

where ρ is the density of the liquid (Ma et al., 2003). Equation (1) assumes that the characteristic velocity for the induced electric field is $(\sigma_L \phi_0 B / \rho)^{1/2}$, which is given by a balance between the EM body force and the nonlinear inertial term in the momentum equation. For the EM stirring in the VGF growth of gallium-antimonide (GaSb) crystals considered by Ma et al. (2003), $\phi_0 = 0.215 mV, B = 0.126 mT, R = 25 mm, \rho = 6030 kg/m^3$ and $\sigma_L = 1.0 MS/m$. Therefore, N=0.0000318, so that the induced electric field can be neglected in Ohm's law.

The dimensionless equations governing the electric potential function ϕ and the electric current density $\mathbf{j}$ are

$$\frac{\partial^2 \phi}{\partial r^2} + \frac{1}{r} \frac{\partial \phi}{\partial r} + \frac{\partial^2 \phi}{\partial z^2} = 0, \tag{2}$$

$$j_r = -\frac{\partial \phi}{\partial r}, \quad j_z = -\frac{\partial \phi}{\partial z}. \tag{3}$$

Here r and z are normalized by R, while ϕ is normalized by ϕ_0, and $\mathbf{j}$ is normalized by $\sigma_L \phi_0 / R$. The boundary conditions are

$$\phi = 1, \text{ at } r = 1, \tag{4}$$

$$\frac{\partial \phi}{\partial z} = 0, \text{ at } z = -b \tag{5}$$

$\phi = 0$, at $z = b$ for $0 \leq r \leq a$, (6)

$\dfrac{\partial \phi}{\partial z} = 0$, at $z = b$ for $a \leq r \leq 1$. (7)

The separation-of-variables solution of the equation (2) and of the boundary conditions (4) and (5) is

$$\phi = 1 + \sum_{N=1}^{NT} A_N J_0\left(\lambda_N r\right) \frac{\cosh\left[\lambda_N\left(z+b\right)\right]}{\cosh\left(2\lambda_N b\right)},$$ (8)

where J_0 is the Bessel function of the first kind and zeroth order, while λ_N are the zeros of J_0. The coefficients A_N are determined by minimizing a residual E based on the boundary conditions (6) and (7),

$$E = \int_0^a r\left[\phi(r,b)\right]^2 dr + w \int_a^1 r\left[\frac{\partial \phi}{\partial z}(r,b)\right]^2 dr.$$ (9)

The weighting factor w is included in order to insure that the errors in both boundary conditions are small. We used $NT = 500$ which gave very small errors for both boundary conditions with a range of values for w, while $w = 0.1$ for the results presented here. The dimensional EM body force in the azimuthal direction is

$$\left(\frac{\sigma_L \phi_0 B}{R}\right)\frac{\partial \phi}{\partial r}.$$ (10)

The dimensionless equations governing the liquid velocity **v** are

$$\frac{\partial \mathbf{v}}{\partial t} + (\mathbf{v} \bullet \nabla)\mathbf{v} = -\nabla p + Tm\frac{\partial \phi}{\partial r}\hat{\theta} + \nabla^2 \mathbf{v},$$ (11)

$$\nabla \bullet \mathbf{v} = 0,$$ (12)

where t is time normalized by R^2/ν, p is pressure normalized by $\rho \nu^2/R^2$, **v** is normalized by ν/R, and ν is the kinematic viscosity of the liquid. The magnetic Taylor number

$$Tm = \frac{\sigma_L \phi_0 B R^2}{\rho \nu^2}$$ (13)

is the dimensionless representation of the azimuthal EM body force. The boundary conditions are

$\mathbf{v} = 0$, at $r = 1$ and at $z = \pm b$. (14)

This paper treats the steady axisymmetric flow driven by the EM body force, but we also want to verify that all

the flows considered here are stable with respect to small disturbances. For each component of the velocity and for the pressure, we introduce the form

$$v_r = v_{r0}(r,z) + \varepsilon\text{Real}\left[v_{r1}(r,z)\exp(\lambda t - im\theta)\right] + O\left(\varepsilon^2\right),$$ (15)

where the subscript 0 denotes the variables for the steady axisymmetric base flow, the subscript 1 denotes the complex modal functions such as $v_{r1} = v_{r1R} + iv_{r1I}$, $\lambda = \lambda_R + i\lambda_I$ is the complex eigenvalue, m is the real integer azimuthal wave number and $\varepsilon \ll 1$. The form given by equation (15) is introduced into equations (11) and (12) and the boundary conditions (14), and $O\left(\varepsilon^2\right)$ terms are neglected. The equations for the steady, axisymmetric base flow are given by the terms without an ε. With the base-flow equations satisfied, the eigenvalue problem for the linear stability analysis is given by the terms with ε.

For the steady axisymmetric base flow, we introduce a stream function $\psi(r,z)$ where

$$v_{r0} = \frac{1}{r}\frac{\partial \psi}{\partial z}, \quad v_{z0} = -\frac{1}{r}\frac{\partial \psi}{\partial r},$$ (16)
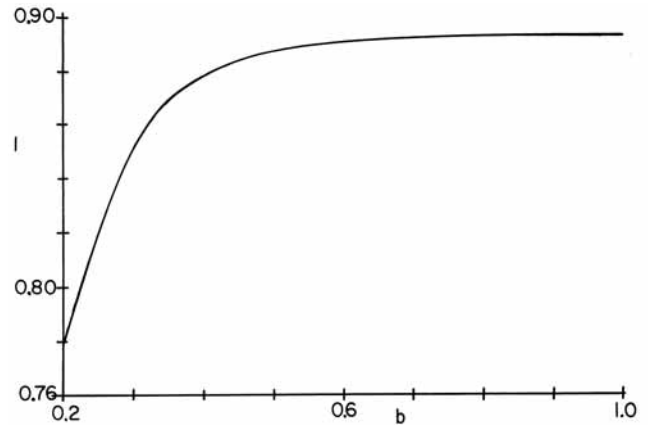

Figure 2 : Total dimensionless electric current versus the aspect ratio of the melt region.

and we eliminate p_0 by cross-differentiating the r and z components of equation (11). Therefore the base flow is governed by a fourth-order equation for ψ and a second-order equation for $v_{\theta 0}$. We represent each of these two base-flow variables by a sum of Chebyshev polynomials in r and z. We insure that the representations have the correct Taylor series in r, i.e., $v_{\theta 0}$ has only odd powers of r, and ψ has only even powers of r, starting with r^2.

We apply each equation at the Gauss-Lobatto collocation points, including $r = 0$. For each equation at $r = 0$, we identify the leading power of r in the Taylor series for that equation, we divide by that power of r, and we take the limit as $r \rightarrow 0$. The nonlinear base-flow equations are solved with an iterative Newton-Raphson scheme.

The complex modal functions $v_{r1}, v_{\theta 1}, v_{z1}, p_1$ are governed by a set of linear homogeneous equations and boundary conditions. The governing equations involve coefficients given by the base-flow variables and their first derivatives, and they also involve the complex eigenvalue λ from the time derivative in equation (11). We use the continuity equation (12) to eliminate $v_{\theta 1}$ and we use the azimuthal component of the momentum equation (11) to eliminate p_1. Therefore we have two fourth-order equations governing v_{r1}, v_{z1}. Each of these perturbation variables is represented by a sum of Chebyshev polynomials in r and z. We insure that each representation has the correct Taylor series in r, i.e., v_{r1} includes $r^{(m-1)}, r^{(m+1)}, r^{(m+3)}, ...,$ and v_{z1} includes $r^m, r^{(m+2)}, r^{(m+4)}, ...$ The perturbation equations are applied at the same Gauss-Lobatto points. Again the leading term in the Taylor series of each equation is applied at $r = 0$. The resultant complex linear matrix eigenvalue problem was solved with the FORTRAN subroutines in the EISPACK library (Smith et al., 1976).

For each combination of the the parameters Tm, b, a, we first use the Newton-Raphson scheme to determine the steady axisymmetric base flow and we then use the EISPACK subroutines to determine all the complex eigenvalues for $m = 1,2,3,4,5,6....$ The base flow is stable with respect to small perturbations if $\lambda_R < 0$ for every eigenvalue for every value of m.

3 Results

The electric potential function ϕ depends on the values of a and b. We only consider $a = 0.2$. For the application treated by Ma et al. (2003), $b = 0.2$. One purpose of this paper is to determine how the flow varies with the aspect ratio b over the range $0.2 \leq b \leq 1.0$. The total dimensionless electric current between the two electrodes is

$$I = 2\pi \int_{-b}^{b} \frac{\partial \phi}{\partial r}(1,z)\,dz. \tag{17}$$

The value of I is plotted as a function of b in Fig. 2.

After increasing from $I = 0.779$ for $b = 0.2$ to $I = 0.877$ for $b = 0.4$, I begins to asymptote to its value for $b = \infty$. For $b > 0.4$, the current is concentrated near $z = b$, so that the electrically insulating boundary at $z = -b$ has very little effect on the electric current.

The dimensionless azimuthal EM body force $\partial \phi / \partial r$ near $z = b$ is larger than that near $z = -b$ for all values of b, but the difference increases rapidly as b is increased from 0.2 to 1.0. The contours of $\partial \phi / \partial r$ for $b = 0.2$ and for $b = 1.0$ are plotted in Fig. 3a and Fig. 3b, respectively. For $b = 0.2$, there is a significant EM body force near $z = -0.2$, with the maximum value at $z = -0.2$ being 0.55. For $b = 1.0$, $\partial \phi / \partial r < 0.2$ for $z < 0.5$ and the maximum value at $z = -1$ is less than 0.01.

The flow depends on a, b and Tm. For the growth of GaSb crystals with $\phi_0 = 0.215mV$, $B = 0.126mT$ and $R = 25mm$, the value of Tm is 19500 (Ma et al., 2003). Here we are interested in the magnitude and characteristics of the steady axisymmetric meridional circulation as functions of b and Tm, so we consider the range $0 \leq Tm \leq 100000$. The azimuthal velocity $v_{\theta 0}$ is driven by the EM body force $Tm\partial \phi / \partial r$ and the meridional circulation is driven by the axial variation of $v_{\theta 0}^2 / r$. Since $v_{\theta 0} = 0$ at $z = \pm b$, there is always radially outward flow in the central part of the melt and radially inward flow near both $z = b$ and $z = -b$. Therefore the meridional circulation always consists of a clockwise circulation with radially inward flow near $z = -b$ and a counterclockwise circulation with radially inward flow near $z = b$. As b is increased from 0.2 to 1.0, the EM body force becomes much more concentrated near $z = b$, as illustrated in Fig. 3, so that we expect the relationship between the two meridional circulations to vary strongly with b. For $Tm = 100000$, the contours of ψ for $b = 0.2$ and for $b = 1.0$ are presented in Fig. 4a and Fig. 4b, respectively. For $Tm = 100000$ and $b = 0.2$, $-4.92 \leq \psi \leq 4.78$, so that the clockwise circulation is only slightly larger than the counterclockwise one, and each occupies roughly half of the melt region. For $Tm = 100000$ and $b = 1.0$, $-16.26 \leq \psi \leq 4.93$, so that the clockwise circulation is much stronger than the counterclockwise circulation, which is confined to the region $0.7 \leq z \leq 1.0$.

The magnitude of the clockwise circulation $-\psi_{\min}$ and the magnitude of the counterclockwise circulation $\psi_{\max}$ are plotted as functions of Tm for $b = 0.2$, 0.5, 0.75 and 1.0 in Figs. 5a and 5b, respectively. As b is increased, the magnitude of the clockwise circulation increases mono-
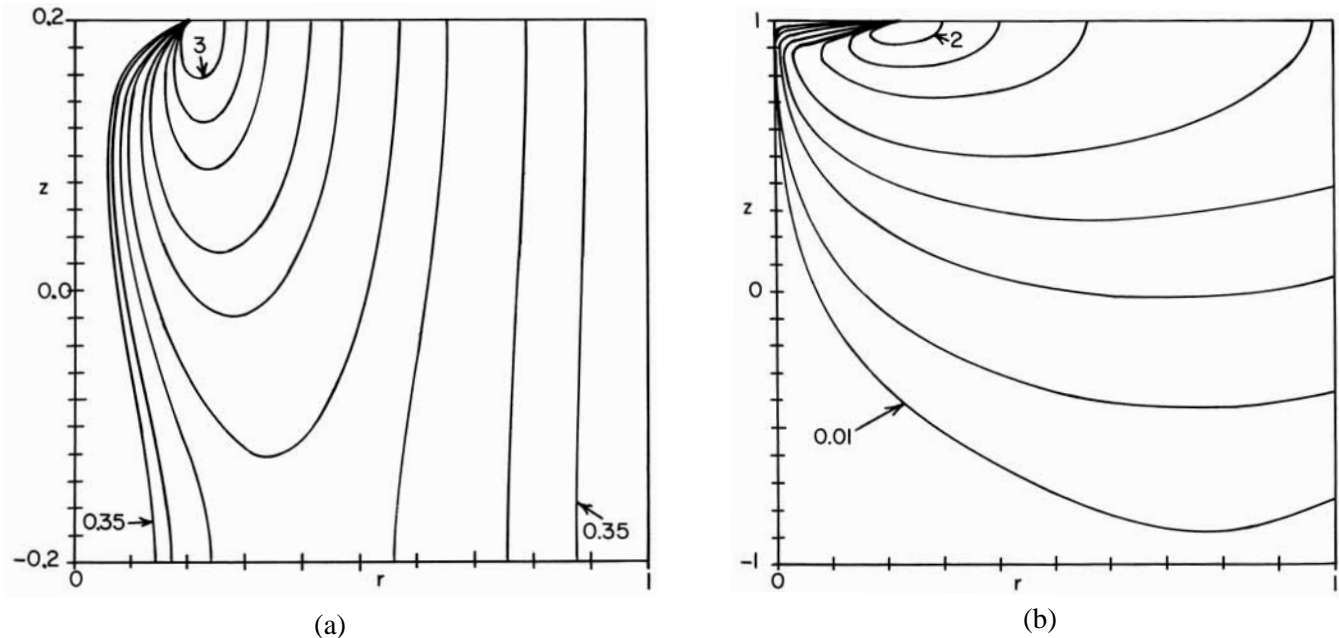
Figure 3 : Dimensionless electromagnetic body force. a. For $b = 0.2$, $\partial\phi/\partial r = 0.35$, 0.4, 0.5, 0.6, 0.8, 1.0, 1.5, 2.0 and 3.0. b. For $b = 1.0$, $\partial\phi/\partial r = 0.01$, 0.02, 0.05, 0.1, 0.2, 0.5, 1.0 and 2.0.
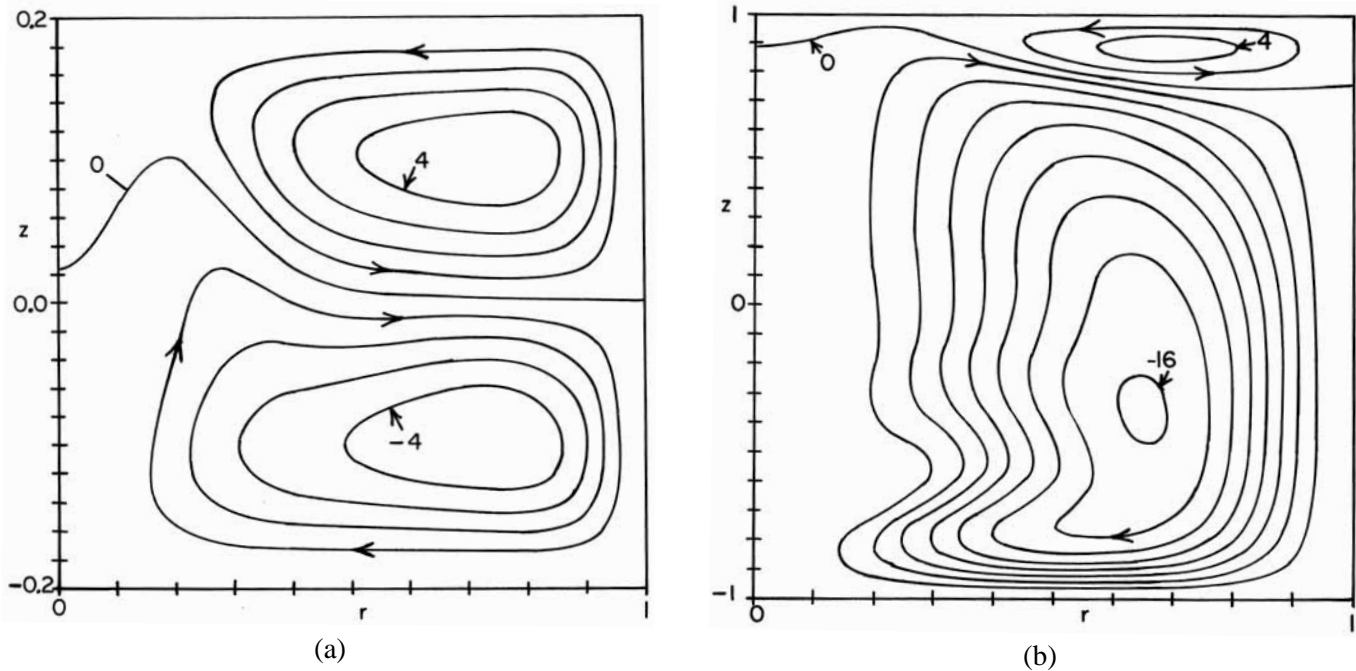

Figure 4 : Streamlines for the dimensionless meridional circulation with $Tm = 100000$. a. For $b = 0.2$, $\psi = k$, for $k = -4$ to 4. b. For $b = 1.0$, $\psi = 2k$, for $k = -8$ to 2.

tonically, but the magnitude of the counterclockwise circulation first increases until it reaches a maximum for $b = 0.5$ and then it decreases.

The maximum value of $v_{\theta 0}$ is plotted as a function of Tm for $b = 0.2$, 0.5, 0.75 and 1.0 in Fig. 6. The varia- tion of $v_{\theta 0\,max}$ with b is smaller than the variation of either the clockwise or counterclockwise meridional circulation. For $Tm < 35000$, the value of $v_{\theta 0\,max}$ decreases monotonically as b is increased from 0.2 to 1.0. For $Tm > 35000$, $v_{\theta 0\,max}$ first increases to a maximum for $b =$
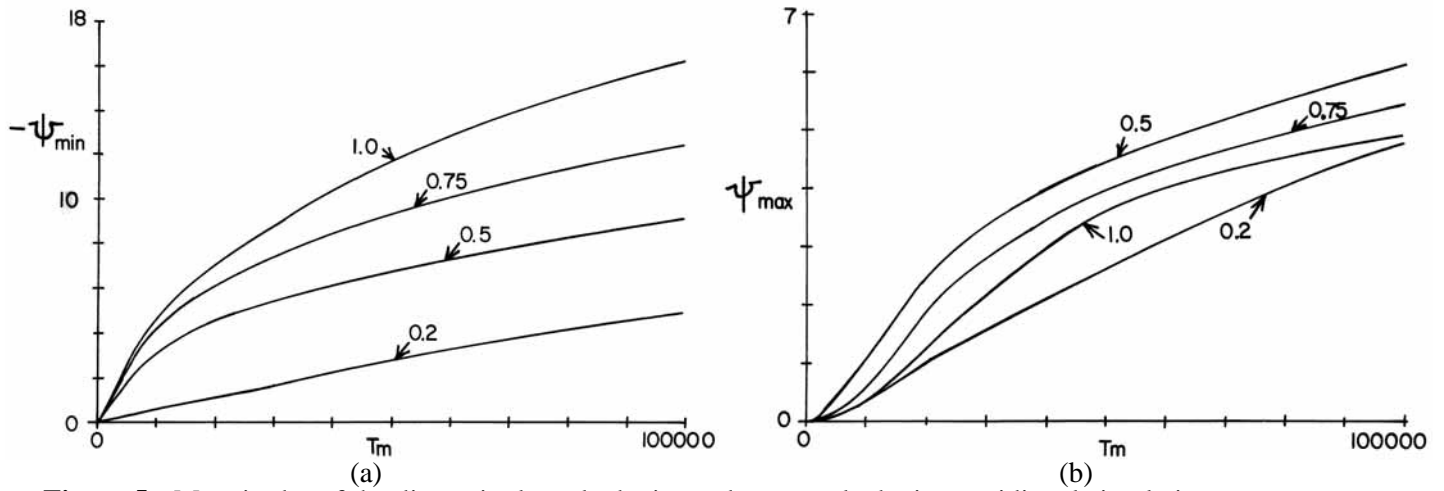
Figure 5 : Magnitudes of the dimensionless clockwise and counterclockwise meridional circulations versus *Tm*. a. Clockwise circulation $-\psi_{min}$. b. Counterclockwise circulation ψ_{max}.
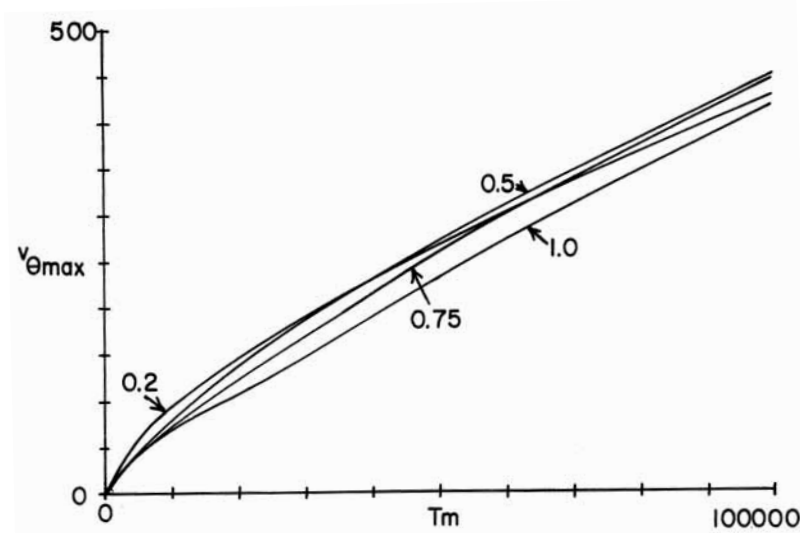

Figure 6 : Maximum dimensionless azimuthal velocity versus *Tm*.

0.5 and then decreases as *b* is increased to 1.0. Davidson (1992) argued that the magnitude of $v_{\theta 0\,max}$ with an azimuthal body force depends on the balance between the addition of angular momentum by the azimuthal body force and the loss of angular momentum due to viscous shear stresses near the boundaries, all during one circuit around each streamline for the meridional circulation. Since *I* is roughly proportional to the total azimuthal force on the fluid, Fig. 2 indicates that the total force increases as *b* is increased from 0.2 to 0.4 and then begins to asymptote to a constant value as *b* is increased further to 1.0. On the other hand, the magnitude of the clockwise meridional circulation increases roughly in proportion to *b*. Therefore, during one circuit around any meridional

streamline, the loss of angular momentum due to viscous stresses increases more than the addition of angular momentum by the azimuthal body force as *b* is increased.

There are two causes for the decrease of the counterclockwise circulation near $z = b$ as *b* is increased from 0.5 to 1.0. First, $v_{\theta 0\,max}$ is decreasing with increasing *b*. Second, the magnitude of the clockwise circulation is increasing, and the associated viscous shear stresses decrease the counterclockwise circulation. The clockwise circulation increases in spite of the small decrease in $v_{\theta 0\,max}$ because the axial extent of the clockwise circulation increases greatly as *b* is increased, while the axial extent of the counterclockwise circulation decreases

slightly.

All of the steady axisymmetric flows considered here are stable with respect to small perturbations.

4 Conclusions

The primary purpose of EM stirring in the VGF process with a submerged heater is to eliminate the radial macrosegregation. The radial distribution of additives in the crystal depends on the characteristics of the meridional flow in the melt. In EM stirring, the meridional flow consists of a clockwise circulation with radially inward flow near the crystal-melt interface and a counterclockwise circulation with radially inward flow near the bottom of the submerged heater. The results presented here show that the magnitudes of both circulations and the relationship between the two circulations depend strongly on the axial distance between the crystal-melt interface and the bottom of the heater. For fixed values of the voltage difference between the two electrodes and of the magnetic field strength, the radial distribution of additives in the crystal will be a strong function of the axial length of the melt region. As a controllable parameter, this axial length provides another method to improve crystal quality.

References

Davidson, P.A. (1992): Swirling flow in an axisymmetric cavity of arbitrary profile, driven by a rotating magnetic field. *J. Fluid Mechanics*, vol. 245, pp. 669-699.

Dold, P.; Benz, K. W. (1999): Rotating magnetic fields: fluid flow and crystal growth applications. *Prog. Cryst. Growth Charact. Mater.*, vol. 38, pp. 7-38.

Grants, I.; Gerbeth, G. (2002): Linear three-dimensional instability of a magnetically driven rotating flow. *J. Fluid Mechanics*, vol. 463, pp. 229-239.

Ma, N.; Bliss, D. F.; Iseler, G. W. (2003): Vertical gradient freezing of doped gallium-antimonide semiconductor crystals using submerged heater growth and electromagnetic stirring. *J. Crystal Growth*, vol. 259, pp. 26-35.

Monberg, E. (1994): *Bridgman and related growth techniques. Handbook of Crystal Growth, vol. 2*, ed. by D. T. J. Hurle, pp. 51-97, Elsevier Science, Amsterdam.

Ostrogorsky, A. G.; Muller, G. (1994): Normal and zonal solidification using the submerged heater method. *J. Crystal Growth*, vol. 137, pp. 64-74.

Smith, B. T. et al. (1976): *Matrix eigensystem routines—EISPACK Guide, 2nd ed.*, vol. 6, Lecture Notes in Computer Science, Springer, NY.

Wang, X.; Ma, N.; Bliss, D. F.; Iseler, G. W.; Becla, P. (2006): Comparing modified vertical gradient freezing with rotating magnetic field or with steady magnetic and electric fields. *J. Crystal Growth*, vol. 287, pp. 270-274.

Watanabe, M.; Eguchi, M.; Hibiya, T. (1999): Silicon crystal growth by the electromagnetic Czochralski (EMCZ) method. *Jpn. J. Appl. Phys.*, vol. 38, pp. L10-L13.

Watanabe, M.; Eguchi, M.; Wang, W.: Hibiya, T.; Kuragaki, S. (2002): Controlling oxygen concentration and distribution in 200 mm diameter Si crystals using the electromagnetic Czochralski (EMCZ) method. *J. Crystal Growth*, vols. 237-239, pp. 1657-1662.